Fabrication and characterization of Ni-Ce-Zr ternary disk-shaped catalyst and its application for low-temperature CO_2 methanation

Dea Hyun Moon[a,1], Woo Jin Chung[b,1], Soon Woong Chang[b,*,1], Sang Moon Lee[b], Sung Su Kim[b], Jae Hoon Jeung[a], Yeon Hee Ro[a], Jeong Yoon Ahn[a], Wenshan Guo[c], Huu Hao Ngo[c], Dinh Duc Nguyen[b,d,*]

[a] *Department of Environmental Energy Engineering, Graduate School of Kyonggi University, Suwon, Republic of Korea*

[b] *Department of Environmental Energy Engineering, Kyonggi University, Suwon, Republic of Korea*

[c] *Centre for Technology in Water and Wastewater, School of Civil and Environmental Engineering, University of Technology Sydney, Sydney, NWS 2007, Australia*

[d] *Institute of Research and Development, Duy Tan University, Da Nang, Vietnam*

[*] Corresponding authors.
E-mail addresses: swchang@kyonggi.ac.kr (S.W. Chang), nguyensyduc@gmail.com (D.D. Nguyen).
[1] These authors contributed equally to this work.

Keywords: Carbon dioxide; Methanation catalyst; Disk-shaped catalyst; Nickel; Cerium; Zirconium

Abstract

This study optimized a Ni-Ce-Zr catalyst and its contents for a CO_2 methanation reaction by selecting a disk shape with a high mechanical strength, good durability, and thermal emission resistance. The physical and chemical properties of the obtained catalysts were determined by X-ray diffraction, scanning electron microscopy, Brunauer–Emmett–Teller, hydrogen temperature-programmed reduction, and temperature-programmed desorption of CO_2 analyses. In addition, the activity and stability of the obtained catalysts were then evaluated and compared. It was determined that the combined Ni-Ce-Zr catalyst positively affects the conversion of CO_2 to CH_4. Furthermore, a CO_2 methanation experi- ment was performed under atmospheric pressure conditions at 200–350 °C. The CO_2 conversion was 82% at 300 °C, and the CH_4 selectivity was 100%. A durability test revealed a difference in the conversion of approximately 6% for 1000 h, which indicates that the catalytic performance was maintained for a significant period.

1. Introduction

In recent years, the issue of reducing greenhouse gas emissions has gained major interest [1]. According to the Fourth Assessment Report published by the Intergovernmental Panel on Climate Change (IPCC) in 2007, carbon dioxide (CO_2) is responsible for most of the global warming observed over the last fifty years. The Fifth Assessment Report (2013) reported that the CO_2 concentration in the atmosphere prior to industrialization was only approximately 280 ppm; however, it increased significantly to 391 ppm in 2011 and to 400 ppm in 2014 [2]. Therefore, the need to significantly reduce CO_2 around the world has increased. Over the years, there have been many attempts to convert CO_2 into a useful resource [3–5], and to solve the above-mentioned problem, various methods for treating and converting CO_2 have been proposed [6]. In the presence of hydrogen, the overall CO_2 methanation reaction converts CO_2 into methane, as presented in the formula below (Eq. (1)). This chemical conversion method is much faster and more effective than methods that convert CO_2 into hydrocarbons, plastics, high-molecule compounds, or alcohols during a reaction [7,8].

$$CO_{2(gas)} + 4H_{2(gas)} \rightarrow CH_{4(gas)} + 2H_2O_{(gas)}, \quad \Delta H = -165.0\ kJ/mol, \quad \Delta G = -113.2\ kJ/mol \tag{1}$$

The mechanism of the CO_2 methanation reaction can be described via the following six-step reaction: [9–11]. First, CO_2 is adsorbed onto the catalyst surface, and it is subsequently dissociated into to CO_{ads} and O_{ads} ($CO_{2ads} \rightarrow CO_{ads} + O_{ads;}$ Step 1); CO_{ads} is then rapidly absorbed and leads to the reactions of $CO_{ads} \rightarrow C_{ads} + O_{ads}$ (Step 2) and $2CO_{ads} \rightarrow C_{ads} + CO_{2gas}$ (Step 3). The dissociation of CO in Step 2 is irreversible due to the sudden removal of surface O_{ads} after hydrogenation, and the dissociation of CO_{ads} in Step 3 occurs by disproportion [12]. Next, the rate-determining steps that lead to the following reactions are completed: $C_{ads} + H_{ads} \rightarrow CH_{ads}$ (Step 4) and $CH_{ads} + H_{ads} \rightarrow CH_{2ads}$ (Step 5). Finally, CH_4 is produced by the reaction of CH_{2ads} with hydrogen as follows: $CH_{2ads} + 2H_{ads} \rightarrow CH_{4gas}$ (Step 6).

The CO_2 methanation reaction can convert CO_2 effectively because it is an exothermic reaction, and it works at low temperatures with respect to thermodynamics [13]. The reaction should be conducted at a temperature of 400 °C or below [14]. Under temperature conditions of 450 °C or above, carbon monoxide (CO) selectivity increases due to the reverse water-gas shift (RWGS) reaction. Therefore, the catalyst is required to achieve a proper reaction rate and methane (CH_4) selectivity [15,16]. Metallic catalysts, such as nickel (Ni) [17], iron (Fe) [18], cerium (Ce) [19], aluminum (Al) [20], silicon (Si) [21], and titanium (Ti) [22], are used in the CO_2 methanation reaction. Studies utilizing precious metals, such as platinum (Pt) [23], palladium (Pd) [24,25], rhodium (Rh) [24], and ruthenium (Ru) [26], have also been reported. Compared with precious metals, nickel-based catalysts exhibit a high activity, methane selectivity and are widely used because of their economic efficiency, availability, etc. [27–29]. The performance and stability of the catalyst are influenced by the characteristics of the metal support used [30] and the interaction between the reactive metals and the support [31,32]. Generally, Ce and zirconium (Zr) are widely used as promoters for Ni support [33]; Ce addition stabilizes the noble metal on the surface of the catalyst and accelerates the reaction with hydrocarbons at low temperature. Moreover, it has the advantage of storing and releasing oxygen due to a high oxygen storage capacity. However, it has low heat stability properties [34,35]. A combined catalyst consisting of Ni, Ce, and Zr improves the catalyst's capacity to store oxygen and demonstrates outstanding activity capability [36,37]. In addition, a combined catalyst consisting of Ni, Ce, and Zr has a high oxida- tion–reduction potential, excellent thermal stability, and resistance to sintering phenomena [38,39]. In the case of Ni calcination, oxygen combines two Ni atoms and forms NiO. The formation of NiO leads to a decrease in Ni grain size and prevents the sintering of particles. It is also known that the catalytic activity increases as the size of the Ni grain decreases. However, the grain size increase and activity site decrease when sintering occurs. Eventually, this leads to a decline in the catalytic activity. The majority of studies have focused on powder catalysts, whereas studies using honeycomb types [9,40] and Ni nanotube types [41,42] have also been reported. However, the practical application of these powdered catalysts to the large-scale system poses difficulties in handling and drawbacks due to low efficiency, complicated operation and management, and high capital costs [13,43]. In addition, to our knowledge, the available information on a combined catalyst consisting of Ni, Ce, and Zr in a disk shape has many limitations and gaps for practical application, requiring adequate investigation to optimize their performance and overcome the aforementioned difficulties.

Hence, the main objectives of this work are: (i) to manufacture a series of Ni-Ce-Zr ternary disk-shaped catalysts with different Zr contents and determine their physico-chemical properties by various technical analyses; (ii) to evaluate and compare the obtained Ni-Ce-Zr catalysts and contents for the CO_2 methanation reaction under conditions of atmospheric pressure and low temperatures of 200–350 °C; and (iii) to verify the stability and durability of the best activity among the disk-shaped catalysts produced for over 1000 h for optimization of the methanation reaction.

2. Materials and methods

2.1. Catalyst preparation

In this study, Ni (99.9%, Nickel powder, Sigma Aldrich Co., USA), Ce (99.9%, cerium (III) nitrate hexahydrate [$Ce(NO_3)_3 \cdot 6H_2O$], Sigma Aldrich Co., USA), and Zr (99.9%, zirconium dioxide [ZrO_2], Sigma Aldrich Co., USA) are used as samples. A physical mixed method was applied to make the catalyst. The Zr content was adjusted to 0%, 10%, 20%, and 30%. The weight of the samples was measured based on the weight ratio, and the catalyst was then mixed with distilled water. The sample was agitated for 1 h at room temperature, and moisture was evaporated in an evaporator (EYELA SB-1100, Changshin Scientific Co., Korea) at 70 °C. Then, the sample was dried for 24 h in a dry oven at 105 °C to remove residual moisture. Large particles were removed by sifting through a 50-μm sieve, and the disk-shaped catalyst was formed under a pressure of 10,000 lbf through a mold (D = 2.54 cm). The prepared catalyst was then heat-treated at 550 °C and at the heating rate of 2 °C/min in an air atmosphere.

2.2. Catalytic activity tests

The equipment used in this study consisted of stainless steel and can be classified into gas injection, reactor, and gas components. The flow rate was adjusted by using a mass flow controller (MFC, Type 1179A, MKS Instruments, Inc., USA). The sample was preheated at 180 °C as it passed through a heat line before entering the main vertical reactor with dimensions of 300 mm width × 300 mm length × 430 mm height, and the reaction had a temperature of 200–350 °C. CO_2, H_2, and ni- trogen (N_2) gases were injected at a ratio of CO_2:H_2:N_2 = 1:4:1. The flow rates were 20 mL, 80 mL, and 20 mL, respectively (total flow rate was 120 mL/min). A chiller was installed at the end of the reactor to remove moisture. Gas chromatography (GC, YL6500 GC system, YL Instruments Co., Ltd., Korea), a thermal conductivity detector (TCD) and Carboxen-1100 (60/80 mesh) were used to analyze the gas produced after the reaction. After confirming that the desired temperature was held constant, the GC measured the gas composition every 15 min for 1 h. The experiment was conducted while decreasing the

temperature gradually from 350 °C. The gas composition was measured once every 1 h and 15 min, and the CO_2 conversion was determined by using the formula below (Eq. (2)):

$$\mathbf{CO_2\ conversion\ (\%)} = \frac{\mathbf{CO_{2(in)}\ (\%)\ CO_{2(out)}\ (\%)}}{\mathbf{CO_{2(in)}\ (\%)}} \times \mathbf{100} \quad (2)$$

2.3. Characterizations

Scanning electron microscopy (SEM), Brunauer–Emmett–Teller (BET), X-ray diffraction (XRD, Rigaku Co., Japan), temperature-programmed reduction of hydrogen (H_2-TPR), and temperature-programmed desorption of CO_2 (CO_2-TPD) analyses were used to examine the physical and chemical properties of the catalyst in this study. The D/Max 2500 V/PC produced by Rigaku Corporation was used to analyze XRD. Copper potassium-alpha (Cu Kα, λ = 1.5056 Å) was used as the radiation source, and the X-ray generator was 18 kW, and 2θ was 20°–80°. Field emission SEM (FESEM, S8820, Hitachi Co., Japan) with energy dispersive X-ray (EDX) analyses were used to ascertain the surface shape and elemental composition of the catalyst. Ni, Ce, and Zr were selected to determine the composition of elements in EDX. Examinations using H_2-TPR and CO_2-TPD were conducted to measure the catalyst's ability to absorb and desorb oxygen. The H_2-TPR analysis was conducted with the temperature increased to 400 °C at the heating rate of 10 °C/min and then maintained for 30 min in an argon (Ar) atmosphere. After that, the temperature was decreased to room temperature and then increased to 800 °C at the heating rate of 10 °C/min under the condition of 30% H_2. For TPD analysis, the temperature was increased up to 300 °C at the heating rate of 2 °C/min and kept for 1 h in Ar atmosphere. The temperature was then reduced to room temperature, and 15% CO_2 was injected, which was absorbed by the catalyst for 1 h. The quantity of CO_2 desorption was measured by increasing the temperature to 600 °C from room temperature at the heating rate of 2 °C/min.

3. Results and discussion

3.1. Catalyst characterization

SEM and EDX analyses were conducted to measure the surface state of the catalyst produced, and the results are presented in Fig. 1 and Table 1. SEM analysis showed that the grain size of the Ni-Ce catalyst without Zr was significant (Fig. 1a and e), while the grain size of the Ni-Ce catalyst with Zr slightly reduced (Fig. 1b–d and f–h). This may be due to the formation of ZrO_2 resulting from oxygen being joined between Zr and Zr. Heat treating a catalyst results in the sintering phenomenon, which refers to tiny particles combining with one another to minimize their surface energy [10] and to become stabilized in terms of thermodynamics [44]. This causes an increase in grain size and a reduction in the air gap and surface area, resulting in a decrease in the catalyst's activity ability [45]. The combination of oxygen with nickel oxide (NiO), cerium oxide (CeO_2), and ZrO_2 provides a bridge among Ni, Ce, and Zr, which prevents sintering and a reduction in grain size. The EDX analysis showed that as Zr content increased, reactive metals were distributed evenly, and the Ni-20%Ce-10%Zr catalyst had the most uniform distribution.

Table 1
EDX analysis of the Ni-Ce-Zr catalysts.

Catalysts	Elemental weight (%)			
	Ni	Ce	Zr	Total
Ni-Ce	77.68	22.32	–	100.00
Ni-Ce-10%Zr	74.08	18.79	7.13	100.00
Ni-Ce-20%Zr	65.18	21.01	13.82	100.00
Ni-Ce-30%Zr	61.14	17.87	20.99	100.00

XRD analysis was conducted to determine the crystal and oxidation state of each element, and the results are presented in Fig. 2. There were Ni peaks at 44° and 52°, and there were NiO crystals at 37°, 43°, 63°, and 76°. The BET surface area and pore diameter of the produced catalyst were also measured. The results of the BET surface area experiments showed that the specific surface area of the catalyst increases with an increase in Zr loading (Table 2). The Ni-Ce-Zn catalysts with Zr loading of 0%, 10%, 20%, and 30% had BET surface areas of 6.45 m^2/g, 9.12 m^2/g, 7.55 m^2/g and 7.90 m^2/g, respectively. The highest specific surface area of the catalysts was observed at a small amount of 10% Zr loading (Ni-Ce-10%Zr, 9.12 m^2/g), whereas for the catalyst with 20% Zr loading or higher, the specific surface area tended to sharply decline. Also, Ni-Ce-10%Zr catalyst showed the highest pore volume (0.0246 cm^3/g) as well as the activation capacity of the catalyst (Fig. 5). At low or moderate Zr loading, a stronger interaction and well-dis- persed state among Ni, Ce, and Zr together may not have caused the formation of agglomerates between them. Compared with reported in

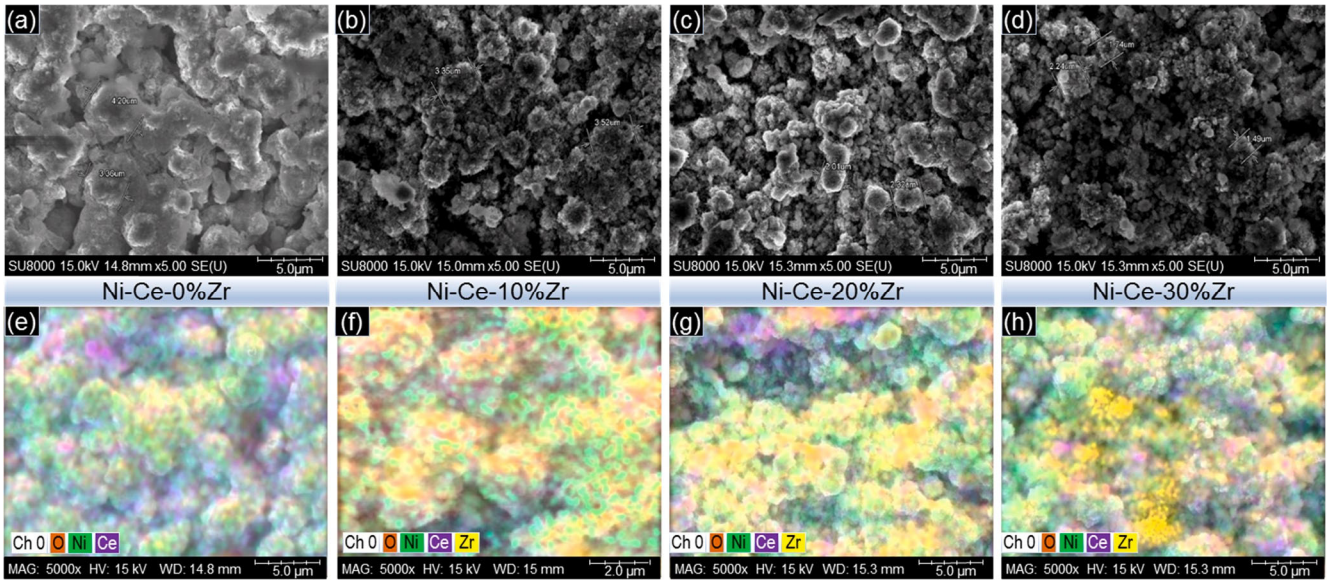

Fig. 1. SEM images (a–d) and EDS mapping images (e–h) of the Ni-Ce-Zr catalyst for different Zr concentrations.

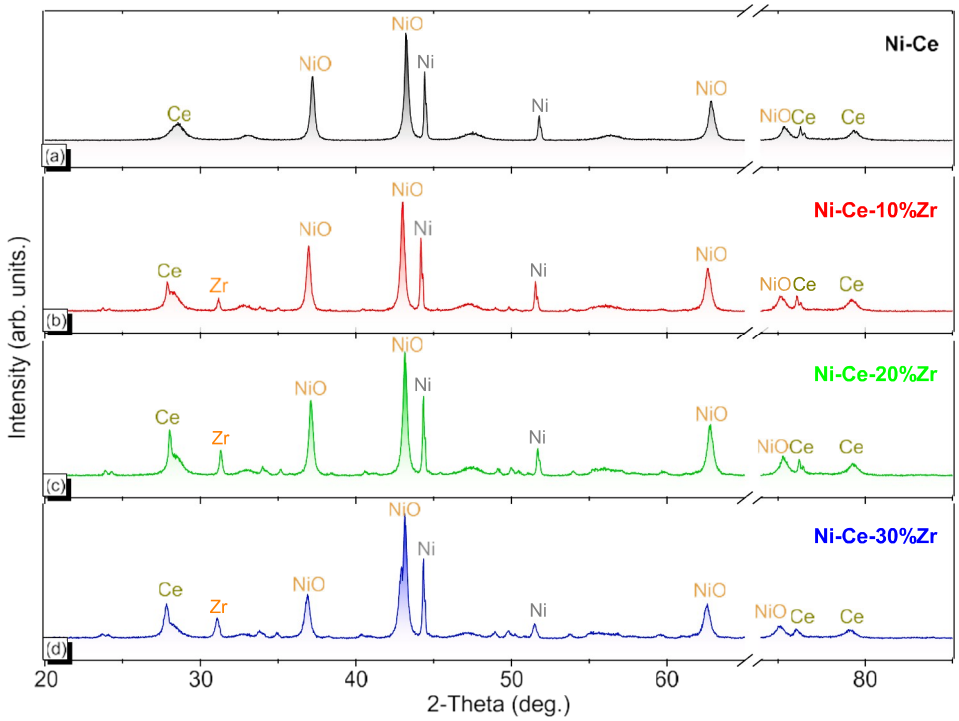

Fig. 2. XRD patterns of the disk-shaped catalysts: (a) Ni-Ce, (b) Ni-Ce-10%Zr, (c) Ni-Ce-20%Zr, and (d) Ni-Ce-30%Zr.

Table 2

BET analysis of the synthesized Ni-Ce-Zr catalysts with different Zr contents.

Catalysts	BET (m^2/g)	Pore volume (cm^3/g)	Nanoparticle size (nm)
Ni-Ce	6.45	0.0221	930.06
Ni-Ce-10%Zr	9.12	0.0246	957.91
Ni-Ce-20%Zr	7.55	0.0159	795.05
Ni-Ce-30%Zr	7.90	0.0180	759.30

the recent literature, the BET specific surface area of the Ni-Ce-Zr disk catalysts prepared in this study are lower than powder catalyst which was reported by Iglesias et al. [33] (60.3–72.9 m^2/g), and Shang et al. [46] (35.1–70.9 m^2/g), because of the disk catalyst was formed under a high pressure (10,000 lbf) through a mold which could lead the particles bonded surfaces together. However, it is noteworthy that even though the prepared catalysts have low specific surface area, but it would perform effectively and stably for the long-term test at low temperatures without undergoing secondary modification such as powder or honeycomb catalysts.

3.2. Effect of Zr content on the catalyst

The H_2-TPR results for the catalyst produced as a function of Zr content are presented in Fig. 3. Two peaks were observed with the first appearing in the range of 250–350 °C. Roh et al. 2002 [47] reported that the first peak is caused by a reduction in CeO_2 and NiO, which means that Ni exists on the surface as NiO. The second peak appeared in the range of 400–500 °C. Graça et al. [9] reported that a peak near 450 °C is caused by the reduction of NiO. Ce-Zr without Ni exhibited a reduction peak near 640 °C [48], and mixing Ce-Zr with Ni lowered the reduction temperature [49]. As a result, hydrogen adsorption capacities on Ni-Ce, Ni-Ce-10%Zr, Ni-Ce-20%Zr, and Ni-Ce-30%Zr were 75.45, 65.06, 60.20 and 59.34, respectively, indicating that the H_2 uptake was reduced by increasing the Zr content.

Zr were carried as results presented in Fig. 4. The result indicates that adsorption capacities of CO_2 on the samples of Ni-Ce, Ni-Ce-10%Zr, Ni-Ce-20%Zr, and Ni-Ce-30%Zr were quite difference, and the Ni-Ce-10% Zr catalyst stability and highest performance for CO_2 adsorption, and as the Zr content increased, CO_2 adsorption decreased.

To evaluate the CO_2 adsorption ability, CO_2-TPD on the prepared catalyst samples of Ni-Ce, Ni-Ce-10%Zr, Ni-Ce-20%Zr, and Ni-Ce-30%

3.3. Catalytic performance

The CO_2 equilibrium conversion and results of the catalytic performance in CO_2 methanation produced under different Zr contents in Ni-Ce-Zr catalysts are presented in Fig. 5. The equilibrium curve was computed from ideal gas phase thermodynamics using a stoichiometric method as described in detail in previous work [50]. The experiment was conducted at 200–350 °C and at a gas hourly space velocity (GHSV) of 14,400 h^{-1}, and for all produced catalysts, the conversion of CO_2 was reduced at a lower reaction temperature. These results show that the Ni-Ce-10%Zr catalyst displayed the best activity, in which the CO_2 conversion attained approximately 82% at 300 °C. With respect to

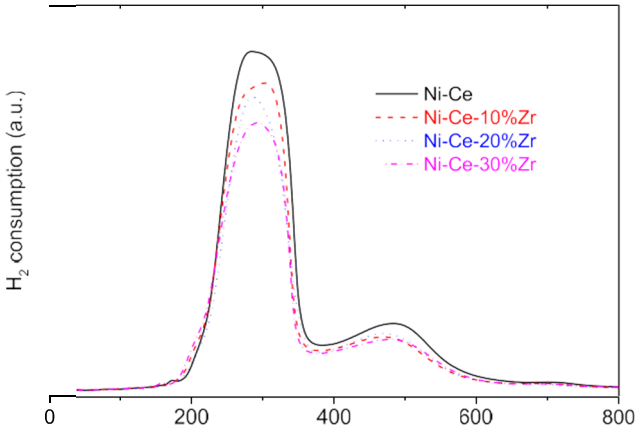

Fig. 3. TPR profiles of the different Ni-Ce-Zr disk-shaped catalyst samples.

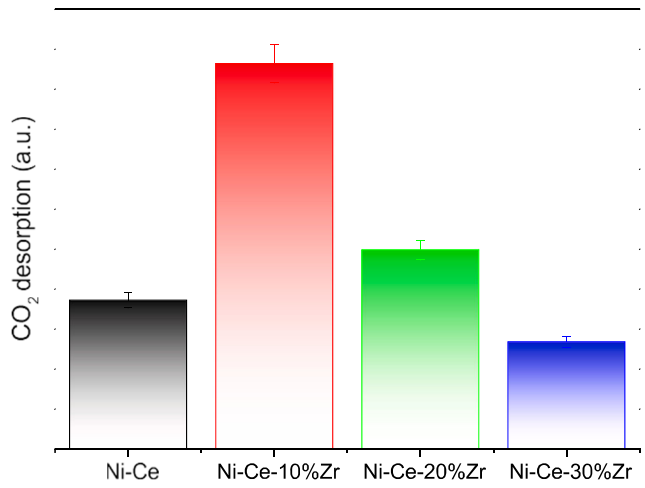

Fig. 4. The maximum desorption of CO_2 for the different Ni-Ce-Zr disk-shaped catalyst samples.

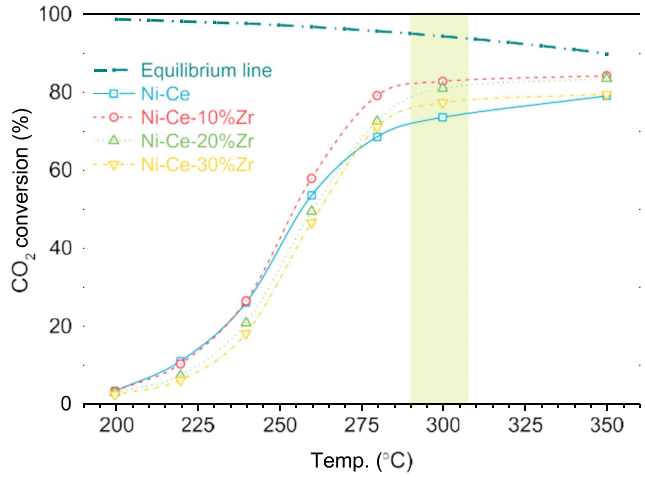

Fig. 5. CO_2 conversions of the Ni-Ce-Zr disk catalysts with different Zr amounts, CO_2:N_2:H_2 = 1:1:4, GHSV: 14,400 h^{-1}, catalyst loading: 3 g, calcined at 550 °C.

activity, these findings represent an improvement, compared to the results reported by Pan et al. [38] (73% CO_2 conversion) and Ocampo et al. [51], and can be explained by the results of the H_2-TPR and CO_2-TPD analyses. It is known that CO_2 methanation reactions show stronger dependence on the H_2 partial pressure than on the CO_2 partial pressure [7,52]. As described previously, as the Zr loading increased, hydrogen consumption decreased, and maximum CO_2 adsorption was observed at 10%Zr. For example, at 300 °C, Ni-Ce was 73%, Ni-Ce-10% Zr was 82%, Ni-Ce-20%Zr was 80%, and Ni-Ce-30%Zr was 77% for the CO_2 conversion, which was similar to CO_2 adsorption. According to the Di Monte, Kašpar [53], when ZrO_2 is added to CeO_2, the oxygen vacancies are increased, and more reduction of Ce-Zr composite was also observed. Therefore, additives such as Ni and Cu can improve the catalytic activity [54,55]. Furthermore, the oxygen storage capacity of CeO_2 on its surface is limited, whereas for Ce-Zr mixed oxides, there is participation of bulk oxygen in the storage process [56]. These results imply that when making a catalyst, there is an optimum ratio of Ni, Ce, and Zr, and this study determined that Ni-Ce-10%Zr is the ideal ratio.

3.4. Catalytic applications

Various form of catalyst was manufactured in optimized contents of the disk type catalyst. Post-treatment such as binder or thermal treatment was excluded in order to figure out the effect of the formation.

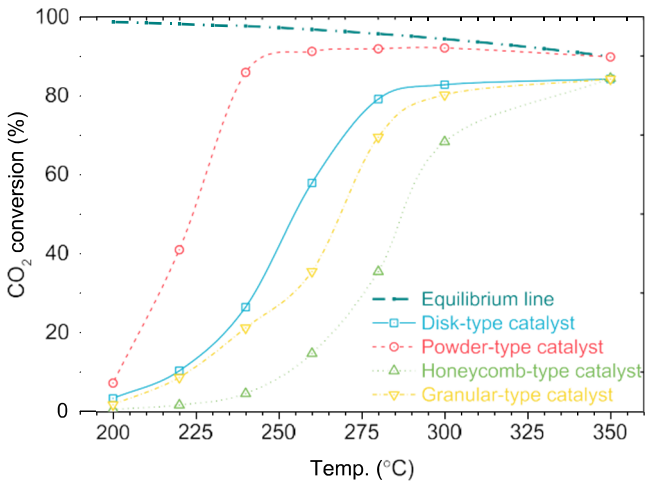

Fig. 6. CO_2 conversions of the Ni-Ce-Zr catalysts with various catalytic form, CO_2:N_2:H_2 = 1:1:4, GHSV: 14,400 h^{-1}.

The reaction characteristics of optimized Ni-20%Ce-10%Zr catalyst in different formation was shown in Fig. 6. The catalyst was formed in powder, honeycomb, disk, and granular types. In these, powder-type catalyst was formed by thermal treatment after the drying process, and granular-type catalyst was manufactured by molding in cylinder with thermal treatment, followed by grinding into 2 mm size. For the honeycomb-type catalyst, distilled water was coated on the catalyst to minimize the effect of binder in 300 cpsi of cell density. In GHSV condition, the powder-type catalyst showed highest activation capacity, whereas honeycomb type catalyst showed the lowest. Generally, powder-type catalyst shows higher activation than modified catalysts because of porosity, bulk density, and BET. In addition, the modified catalysts show sintering phenomenon in the thermal treatment process at high pressure. However, powder-type catalyst has to be modified for the plant scale application, and the catalyst layer has to be cooled as the methanation reaction is an exothermic reaction. If there is not any cooling system in the methanation process, the temperature in the reactor would increase and lead to continuous decrease of the conversion rate. Thus, it is appropriate to apply catalysts with effective cooling formation. In addition, deactivation derived from the exothermic reaction was not found obviously in laboratory experiments. However, when the size of reactor and the amount of CO_2 increase, cooling system equipped is required.

3.5. Stability tests

We conducted a stability test on the Ni-Ce-10%Zr catalyst, which exhibited the best activity among the catalysts produced, and the results are presented in Fig. 7. The reaction temperature was set to 260 °C, which resulted in a conversion efficiency of 50% or higher. The GHSV was conducted under the conditions of 14,400 h^{-1} and atmospheric pressure. The experiment showed that the initial conversion efficiency was 56%, which reduced to 51% after 500 h and was 50% after 1000 h. The catalytic activity declined slightly after a long-term test, which could possibly be due to the byproducts that formed in situ, such as water vapor, and/or the changes in the catalyst structure [57]. This implies that the performance of the catalyst was maintained for a significant period of time without any obvious deactivation, meaning its exhibited a significantly longer, more stable, and efficient performance compared with those reported in previous studies, such as stabilities of 150 h [58] and 140 h [57]. It was therefore confirmed that the disk-shaped catalyst synthesized in this study shows catalytic stability over 1000 h during the reaction. The catalyst manufactured in this study showed outstanding CO_2 conversion and stability. CO_2, the greater part of greenhouse gases, could be effectively reduced. In addition, reactor

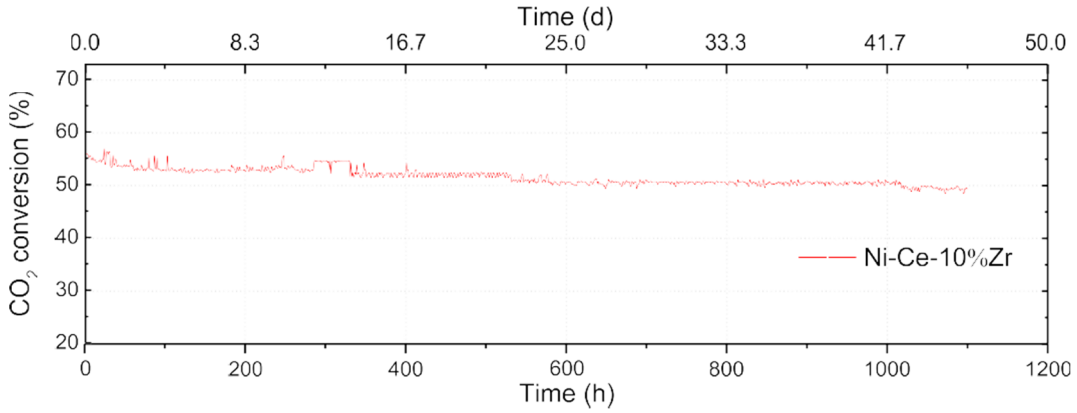

Fig. 7. During the reaction test of the Ni-Ce-10%Zr disk catalyst at constant reaction conditions of CO_2:N_2:H_2 = 1:1:4, GHSV: 14,400 h^{-1}, T = 260 °C.

design is one of the most important factors for consideration. Considering the thermal energy of CO_2 methanation reaction is applied to the catalyst of this study, it will be a promising application of the methanation process.

4. Conclusions

A series of Ni-Ce-Zr ternary disk-shaped catalysts were successfully manufactured using simple mixed method and tested for the CO_2 methanation reaction at low temperatures to confirm their excellent catalytic performance and price competitiveness. The Ni-Ce-Zr catalyst was distributed with reactive metals evenly, which successfully prevented the occurrence of the sintering phenomenon. In addition, Ce-Zr composite catalytic material increased the oxygen storage capacity of the catalyst. The highest CO_2 conversion was found to be approximately 82% under optimized conditions of the Ni-20%Ce-10%Zr catalyst and 300 °C. In various form of catalysts at the same contents, powder type catalyst showed the highest performance, followed by disk, granule and honeycomb type. The durability test of over 1000 h verified that the catalytic performance and activity were maintained for a long period. Therefore, many critical advances were shown, suggesting that the prepared catalyst can potentially be used in industrial applications for the CO_2 methanation.
[15]

Acknowledgements

This work was supported in part by grants from the Korea Institute of Energy Technology Evaluation and Planning (KETEP) and the Ministry of Trade, Industry & Energy (MOTIE) of the Republic of Korea (Project No.: 20183020141270) and the Korean Ministry of Environment as a “Global Top Project” (Project No.: 2016002200005).

Appendix A. Supplementary data

Supplementary data to this article can be found online at https://doi.org/10.1016/j.fuel.2019.116260.

References

[1] Li J-R, Ma Y, McCarthy MC, Sculley J, Yu J, Jeong H-K, et al. Carbon dioxide capture-related gas adsorption and separation in metal-organic frameworks. Coordin Chem Rev 2011;255(15–16):1791–823.
[2] Yue T-X, Zhao M-W, Zhang X-Y. A high-accuracy method for filling voids on remotely sensed XCO_2 surfaces and its verification. J Cleaner Prod 2015;103:819–27.
[3] Centi G, Cum G, Fierro J, Nieto JL. Direct conversion of methane, ethane, and carbon dioxide to fuels and chemicals. Spring House: The Catalyst Group Resources Inc.; 2008.
[4] Ampelli C, Perathoner S, Centi G. CO_2 utilization: an enabling element to move to a resource-and energy-efficient chemical and fuel production. Phil Trans R Soc A 2015;373(2037):20140177.
bi-component Ni-Co catalyst: the anti-carbon deposition and stability of catalyst. Fuel 2019;235:868–77.
[6] Lee S, Lee YH, Moon DH, Ahn JY, Nguyen DD, Chang SW, et al. Reaction mechanism and catalytic impact of Ni/CeO_{2-X} catalyst for low temperature CO_2 methanation. Ind Eng Chem Res 2019.
[7] Ocampo F, Louis B, Kiwi-Minsker L, Roger A-C. Effect of Ce/Zr composition and noble metal promotion on nickel based $CexZr_1-xO_2$ catalysts for carbon dioxide methanation. Appl Catal A-Gen 2011;392(1–2):36–44.
[8] Yamasaki M, Komori M, Akiyama E, Habazaki H, Kawashima A, Asami K, et al. CO_2 methanation catalysts prepared from amorphous Ni–Zr–Sm and Ni–Zr–misch metal alloy precursors. Mater Sci Eng-A 1999;267(2):220–6.
[9] Graça I, González LV, Bacariza MC, Fernandes A, Henriques C, Lopes JM, et al. CO_2 hydrogenation into CH_4 on NiHNaUSY zeolites. Appl Catal B-Environ 2014;147:101–10.
[10] Moon DH, Lee SM, Ahn JY, Nguyen DD, Kim SS, Chang SW. New Ni-based quaternary disk-shaped catalysts for low-temperature CO2 methanation: fabrication, characterization, and performance. J Environ Manage 2018;218:88–94.
[11] Ahn JY, Chang SW, Lee SM, Kim SS, Chung WJ, Lee JC, et al. Developing Ni-based honeycomb-type catalysts using different binary oxide-supported species for synergistically enhanced CO_2 methanation activity. Fuel 2019;250:277–84.
[12] Choe S-J, Kang H-J, Kim S-J, Park S-B, Park D-H, Huh D-S. Adsorbed carbon formation and carbon hydrogenation for CO_2 methanation on the Ni (111) surface: ASED-MO study. B Kor Chem Soc 2005;26(11):1682–8.
[13] Frey M, Romero T, Roger A-C, Edouard D. Open cell foam catalysts for CO_2 methanation: presentation of coating procedures and in situ exothermicity reaction study by infrared thermography. Catal Today 2016;273:83–90.
[14] Kiewidt L, Thöming J. Predicting optimal temperature profiles in single-stage fixed-bed reactors for CO_2-methanation. Chem Eng Sci 2015;132:59–71.
Goodman DJ. Methanation of carbon dioxide Master of Science UCLA: University of California, Los Angeles; 2013.
[16] Jwa E, Lee S, Lee H, Mok Y. Plasma-assisted catalytic methanation of CO and CO_2
[5] Wu H, Liu J, Liu H, He D. CO_2 reforming of methane to syngas at high pressure over

over Ni–zeolite catalysts. Fuel Process Technol 2013;108:89–93.
[17] Rahmani S, Rezaei M, Meshkani F. Preparation of highly active nickel catalysts supported on mesoporous nanocrystalline γ-Al_2O_3 for CO_2 methanation. J Ind Eng Chem 2014;20(4):1346–52.
[18] Schoder M, Armbruster U, Martin A. Heterogeneously catalyzed hydrogenation of carbon dioxide to methane at increased reaction pressures. Chem-Ing-Tech 2013;85(3):344–52.
[19] Xu J, Lin Q, Su X, Duan H, Geng H, Huang Y. CO_2 methanation over TiO_2–Al_2O_3 binary oxides supported Ru catalysts. Chinese J Chem Eng 2016;24(1):140–5.
[20] Razzaq R, Zhu H, Jiang L, Muhammad U, Li C, Zhang S. Catalytic methanation of CO and CO_2 in coke oven gas over Ni–Co/ZrO_2–CeO_2. Ind Eng Chem Res 2013;52(6):2247–56.
[21] Da Silva DC, Letichevsky S, Borges LE, Appel LG. The Ni/ZrO_2 catalyst and the methanation of CO and CO_2. Int J Hydrogen Energy 2012;37(11):8923–8.
[22] Ren J, Qin X, Yang J-Z, Qin Z-F, Guo H-L, Lin J-Y, et al. Methanation of carbon dioxide over Ni–M/ZrO2 (M= Fe Co, Cu) catalysts: effect of addition of a second metal. Fuel Process Technol 2015;137:204–11.
[23] Kim HY, Lee HM, Park J-N. Bifunctional mechanism of CO_2 methanation on Pd-MgO/SiO_2 catalyst: independent roles of MgO and Pd on CO_2 methanation. J Phys Chem C 2010;114(15):7128–31.
[24] Karelovic A, Ruiz P. Mechanistic study of low temperature CO_2 methanation over Rh/TiO_2 catalysts. J Catal 2013;301:141–53.
[25] Sharma S, Hu Z, Zhang P, McFarland EW, Metiu H. CO_2 methanation on Ru-doped ceria. J Catal 2011;278(2):297–309.
[26] Janke C, Duyar M, Hoskins M, Farrauto R. Catalytic and adsorption studies for the hydrogenation of CO_2 to methane. Appl Catal B-Environ 2014;152:184–91.
[27] Taheri Najafabadi A. CO_2 chemical conversion to useful products: an engineering insight to the latest advances toward sustainability. Int J Energy Res 2013;37(6):485–99.
[28] Hwang S, Lee J, Hong UG, Seo JG, Jung JC, Koh DJ, et al. Methane production from carbon monoxide and hydrogen over nickel–alumina xerogel catalyst: effect of nickel content. J Ind Eng Chem 2011;17(1):154–7.

[29] Hwang S, Lee J, Hong UG, Jung JC, Koh DJ, Lim H, et al. Hydrogenation of carbon monoxide to methane over mesoporous nickel-M-alumina (M= Fe, Ni Co, Ce, and La) xerogel catalysts. J Ind Eng Chem 2012;18(1):243–8.

[30] Chang F-W, Kuo M-S, Tsay M-T, Hsieh M-C. Hydrogenation of CO_2 over nickel catalysts on rice husk ash-alumina prepared by incipient wetness impregnation. Appl Catal A-Gen 2003;247(2):309–20.

[31] Zhang J, Xin Z, Meng X, Tao M. Synthesis, characterization and properties of anti-sintering nickel incorporated MCM-41 methanation catalysts. Fuel 2013;109:693–701.

[32] Chung WJ, Nguyen DD, Bui XT, An SW, Banu JR, Lee SM, et al. A magnetically separable and recyclable Ag-supported magnetic TiO_2 composite catalyst: fabrication, characterization, and photocatalytic activity. J Environ Manage 2018;213:541–8.

[33] Iglesias I, Quindimil A, Mariño F, De-La-Torre U, González-Velasco JR. Zr promotion effect in CO_2 methanation over ceria supported nickel catalysts. Int J Hydrogen Energy 2019;44(3):1710–9.

[34] Hori CE, Permana H, Ng KYS, Brenner A, More K, Rahmoeller KM, et al. Thermal stability of oxygen storage properties in a mixed CeO_2-ZrO_2 system. Appl Catal B-Environ 1998;16(2):105–17.

[35] Fornasiero P, Dimonte R, Rao GR, Kaspar J, Meriani S, Trovarelli A, et al. Rh-loaded CeO2-ZrO2 solid-solutions as highly efficient oxygen exchangers: dependence of the reduction behavior and the oxygen storage capacity on the structural-properties. J Catal 1995;151(1):168–77.

[36] Nizio M, Albarazi A, Cavadias S, Amouroux J, Galvez ME, Da Costa P. Hybrid plasma-catalytic methanation of CO_2 at low temperature over ceria zirconia supported Ni catalysts. Int J Hydrogen Energy 2016;41(27):11584–92.

[37] Lu H, Yang X, Gao G, Wang J, Han C, Liang X, et al. Metal (Fe Co, Ce or La) doped nickel catalyst supported on ZrO2 modified mesoporous clays for CO and CO2 methanation. Fuel 2016;183:335–44.

[38] Pan Q, Peng J, Sun T, Gao D, Wang S, Wang S. CO_2 methanation on Ni/Ce0. 5Zr0. $5O_2$ catalysts for the production of synthetic natural gas. Fuel Process Technol 2014;123:166–71.

[39] Strobel R, Krumeich F, Pratsinis SE, Baiker A. Flame-derived Pt/Ba/$Ce_xZr_{1-x}O_2$: influence of support on thermal deterioration and behavior as NO_x storage-reduction catalysts. J Catal 2006;243(2):229–38.

[40] Liu H, Zou X, Wang X, Lu X, Ding W. Effect of CeO_2 addition on Ni/Al_2O_3 catalysts for methanation of carbon dioxide with hydrogen. J Nat Gas Chem 2012;21(6):703–7.

[41] Fukuhara C, Hayakawa K, Suzuki Y, Kawasaki W, Watanabe R. A novel nickel-based structured catalyst for CO_2 methanation: a honeycomb-type Ni/CeO_2 catalyst to transform greenhouse gas into useful resources. Appl Catal A-Gen 2017;532:12–8.

[42] Fukuhara C, Hyodo R, Yamamoto K, Masuda K, Watanabe R. A novel nickel-based catalyst for methane dry reforming: a metal honeycomb-type catalyst prepared by sol–gel method and electroless plating. Appl Catal A-Gen 2013;468:18–25.

[43] Nhut J-M, Vieira R, Pesant L, Tessonnier J-P, Keller N, Ehret G, et al. Synthesis and catalytic uses of carbon and silicon carbide nanostructures. Catal Today 2002;76(1):11–32.

[44] Frontera P, Macario A, Ferraro M, Antonucci P. Supported catalysts for CO_2 methanation: a review. Catalysts 2017;7(2):59.

[45] Lechkar A, Barroso Bogeat A, Blanco G, Pintado JM, Soussi el Begrani M. Methanation of carbon dioxide over ceria-praseodymia promoted Ni-alumina catalysts. Influence of metal loading, promoter composition and alumina modifier. Fuel 2018;234:1401–13.

[46] Shang X, Deng D, Wang X, Xuan W, Zou X, Ding W, et al. Enhanced low-temperature activity for CO_2 methanation over Ru doped the Ni/$Ce_xZr_{(1-x)}O_2$ catalysts prepared by one-pot hydrolysis method. Int J Hydrogen Energy 2018;43(14):7179–89.

[47] Roh HS, Jun KW, Dong WS, Chang JS, Park SE, Joe YI. Highly active and stable Ni/Ce–ZrO_2 catalyst for H_2 production from methane. J Mol Catal A-Chem 2002;181(1–2):137–42.

[48] Dong WS, Roh HS, Jun KW, Park SE, Oh YS. Methane reforming over Ni/Ce-ZrO_2 catalysts: effect of nickel content. Appl Catal A-Gen 2002;226(1–2):63–72.

[49] Koubaissy B, Pietraszek A, Roger A, Kiennemann A. CO_2 reforming of methane over Ce-Zr-Ni-Me mixed catalysts. Catal Today 2010;157(1–4):436–9.

[50] Leal AMM, Blunt MJ, LaForce TC. A robust and efficient numerical method for multiphase equilibrium calculations: application to CO_2–brine–rock systems at high temperatures, pressures and salinities. Adv Water Resour 2013;62:409–30.

[51] Ocampo F, Louis B, Lioubov KM, Roger AC. Effect of Ce/Zr composition and noble metal promotion on nickel based Ce_xZr_1–xO_2 catalysts for carbon dioxide methanation. Appl Catal A 2011;392(1–2):36–44.

[52] Yang Lim J, McGregor J, Sederman AJ, Dennis JS. Kinetic studies of CO2 methanation over a Ni/γ-Al2O3 catalyst using a batch reactor. Chem Eng Sci 2016;141:28–45.

[53] Di Monte R, Kašpar J. Nanostructured CeO_2–ZrO_2 mixed oxides. J Mater Chem 2005;15(6):633–48.

[54] Montini T, Melchionna M, Monai M, Fornasiero P. Fundamentals and catalytic applications of CeO_2-based materials. Chem Rev 2016;116(10):5987–6041.

[55] Kacimi S, Barbier J, Taha R, Duprez D. Oxygen storage capacity of promoted Rh/CeC_2 catalysts. Exceptional behavior of RhCu/CeO_2. Catal Lett 1993;22(4):343–50.

[56] Madier Y, Descorme C, Le Govic AM, Duprez D. Oxygen mobility in CeO_2 and $Ce_xZr_{(1-x)}O_2$ compounds: study by CO transient oxidation and 18O/16O isotopic exchange. J Phys Chem B 1999;103(50):10999–1006.

[57] Marocco P, Morosanu EA, Giglio E, Ferrero D, Mebrahtu C, Lanzini A, et al. CO_2 methanation over Ni/Al hydrotalcite-derived catalyst: experimental characterization and kinetic study. Fuel 2018;225:230–42.

[58] Ocampo F, Louis B, Roger A-C. Methanation of carbon dioxide over nickel-based $Ce_{0.72}Zr_{0.28}O_2$ mixed oxide catalysts prepared by sol–gel method. Appl Catal A-Gen 2009;369(1–2):90–6.